



TECHNICAL ARTICLE

Corrosion Behavior of EN18 Steel and Copper in the Sulfuric Acid Medium for As-Bought and Annealed Materials

Jilna Jomy, Sathyashankara Sharma, P.R. Prabhu, and Deepa Prabhu

Submitted: 14 June 2022 / Revised: 19 October 2022 / Accepted: 19 November 2022 / Published online: 22 December 2022

EN18 steel and copper are used as materials for oil and gas industries for chemical storage, which come in contact with the sulfuric acid medium during the pickling process. In such instances cleaning of impurities and oxide layer removal, leads to excessive corrosion. Thus, the improvement in the microstructure through annealing treatment and its effect on the corrosion behavior of EN18 steel and copper are studied by immersing in 0.5 M H₂SO₄ for as-bought and 0.5, 0.25, 0.1 M H₂SO₄ medium solutions after annealing treatment. The metal specimens were heated to 900 °C for EN18 steel and 600 °C for copper and then both were furnace cooled and the change in the microstructure of annealed and as-received metal specimens was analyzed using Scanning Electron microscopy (SEM). The Electrochemical Impedance Spectroscopy (EIS) and Potentiodynamic polarization (PDP) measurement showed that there is a decrease in the corrosion rate for both metals after annealing treatment. The effect of corrosion rate at the temperature range of 30–50 °C was analyzed and activation parameters were described using Arrhenius and transition state theories. Suitable corrosion mechanisms for both steel and copper in the H₂SO₄ medium have been discussed.

Keywords annealing, copper, corrosion behavior, EIS, EN18 steel, H₂SO₄ medium, PDP, SEM

1. Introduction

Various physicochemical changes that occur in the environment lead to degradation of the metal that leads to corrosion of metal. There are huge economic losses involved in the corrosion process and is considered a huge loss for the infrastructure of various industries. Steel is one of the most widely used engineering materials in pipelines for water and petroleum products. Copper is used in the manufacture of shafts, nuts, and other parts in the chemical storage industry. In these industries, several mineral acids are involved in various treatment processes like acid descaling, acid pickling, and acidifying oil wells (Ref 1). Thus, the degradation of various parts, particularly in acidic environments, has continued to become a high priority for researchers to find a lasting solution to the problem.

In various industries involving these acid treatments, EN18 steel and copper are some of the most commonly used materials. Dual-phase steel finds huge applications in industries due to its mechanical characteristics. Once such dual-phase steel is EN18. EN18 steel consists of pearlite embedded in a ferrite matrix. EN18 steel is considered a base material for various civil infrastructures and chemical storage industries due to its ferrite-pearlite phases, which have the characteristic property of machinability and workability. Copper is considered a common non-ferrous metal used in industries. It has characteristic properties such as good electrical conductivity, workability, and malleability (Ref 2–4). Thus, copper is a good candidate for use in pipeline and oil and gas industries, where acids are commonly used for different treatments (Ref 5).

The microstructure and chemical composition of the metal plays a key role in determining the corrosion property of a metal. The inhomogeneity in the microstructure arises due to the presence of different elemental compositions, and mechanical properties of the material as reported by Clover et al. (Ref 6). Due to the heterogeneities of the metal, small areas act as micro-galvanic cells, where the difference in potential arises (Ref 7).

Heat treatment techniques such as normalizing, annealing, tempering, and hardening are used to modify the microstructure, corrosion, and mechanical properties of metals (Ref 8–11). Heat treatment involved subsequent heating below the recrystallization temperature followed by quenching and tempering to obtain the desired mechanical and corrosion properties (Ref 12, 13). During this process, the metals undergo crystallographic changes including phase changes that affect the physical and mechanical properties of the metals (Ref 14). One such type of heat treatment is annealing. During annealing, the metal is heated to a specific temperature and cooled slowly. During this

Jilna Jomy, Department of Chemistry, Manipal Institute of Technology, Manipal Academy of Higher Education, Manipal, Karnataka 576104, India; **Sathyashankara Sharma**, Department of Mechanical & Manufacturing Engineering, Manipal Institute of Technology, Manipal Academy of Higher Education, Manipal, Karnataka 576104, India; **P.R. Prabhu**, Department of Mechatronics, Manipal Institute of Technology, Manipal Academy of Higher Education, Manipal, Karnataka 576104, India; and **Deepa Prabhu**, Department of Chemistry, International Center for Applied Sciences, Manipal Academy of Higher Education, Manipal, Karnataka 576104, India. Contact e-mail: deepa.prabhu@manipal.edu.

Table 1 Chemical composition of EN18 steel and copper

Metal		Elements and their composition								
EN18 steel	Element	Fe	C	Si	Mn	Al	S	Cr	Ni	Cu
	Composition (wt.%)	96.7	0.37	0.275	0.78	0.032	0.110	0.840	0.166	0.301
Copper	Element	Cu	Zn	Si	P	Fe	Ni	As	Mn	B
	Composition (wt.%)	99.6	0.15	0.018	0.013	0.003	0.0006	0.002	0.0059	0.002

process, recrystallization causes grain growth and leads to the formation of newer grains.

Several studies have reported that by varying the modes of heat treatment, the corrosion resistance of metals can be improved (Ref 15, 16). Zang et al. found out that dual-phase steel has greater corrosion resistance than as-received weathering steel (Ref 17). Kayali et al. investigated the corrosion resistance of ferrite pearlite steel and found out that it has a lower corrosion rate than bronzed steel (Ref 18). D.P. Field et al. have analyzed the change in the microstructure of copper during annealing treatment. It was found that the formation of annealing twins during recrystallization is the driving force for grain growth for copper (Ref 19). The interrelation of the grain size and corrosion property was established by Gaetano et al. It was found that the grain refinement resulted in a decrease in corrosion resistance (Ref 20).

Y. Zaou et al. established the relationship between the microstructure and the corrosion behavior of copper. It was found that the greater the formation of nanotwins greater the corrosion resistance (Ref 21). Oğuzhan Keleştemur et al. analyzed the effect of various heat treatment methods for ferrite-pearlite steel and found that the morphology of the phase substituents had a definite effect on the corrosion resistance of steel (Ref 22). Prvan Kumar Katiyar et al. compared the corrosion behavior of different microstructures of steel such as pearlite, bainite, and martensite and found that the variation in the corrosion rate is due to the variation in the distribution of ferrite and cementite microstructures of the steel. (Ref 23) Although there is literature establishing the relationship between the microstructure and corrosion behavior of steel, the effect of heat treatment of EN18 steel in 0.5 M H₂SO₄ is not studied extensively. The relation between the formation of annealing twins and the corrosion behavior is also studied but the detailed corrosion behavior of copper under various temperature conditions in 0.5 M H₂SO₄ is not well established. Due to the complexity of the mechanism involved in understanding the corrosion behavior of metal, each metal with a slight change in the composition behaves differently. Therefore, in this work, we have analyzed the change in the corrosion resistance properties of EN18 steel and copper in the H₂SO₄ medium before and after annealing treatment.

2. Methodology

2.1 Material Preparation and Annealing Process

EN18 steel and copper are used as the metal substrates for the experiment, and the chemical composition is tabulated in Table 1. The test specimens were made into a cylindrical rod shape of diameter 19 mm and a height of 8 mm. Cleaning and

polishing of the specimen were carried out using emery sheets (80-800) and diamond paste (3-0.25 microns). The prepared specimens are then washed with double distilled water and acetone and dried.

To prepare the annealed samples, EN18 steel was heated in a muffle furnace to a specified austenitization temperature of 900 °C for a period of 2 h (Fig. 1a). The copper specimen is heated in a muffle furnace at 600 °C for a period of 2 h. Thereafter both the samples were furnace cooled to get annealed EN18 steel and annealed copper.

2.2 Medium Preparation

A stock solution of the medium was prepared using analytical grade (Loba Chemie Pvt. Ltd) H₂SO₄ medium (85%) and double distilled water followed by standardization. H₂SO₄ medium of concentrations 0.5, 0.25, and 0.1 M was prepared by appropriate dilution.

2.3 Electrochemical Impedance Spectroscopy (EIS) and Potentiodynamic Polarization (PDP) Method

0.8 and 1.2 cm², respectively, are the exposed area of EN18 steel and copper specimens, that were used as the working electrode. A three-electrode assembly of the working electrode, counter electrode (platinum), and reference electrode (calomel) was immersed in 0.5 M H₂SO₄ for as-bought and 0.5, 0.25, 0.1 M H₂SO₄ medium solutions after annealing treatment. This is connected to a potentiostat (CH600E) and measurements were taken under aerated unstirred conditions at different temperatures (30-50 °C). Each experiment was repeated and triplicated to ensure reproducibility. For EIS measurements, a frequency range of 100 Hz-10 mHz and an amplitude of 10 mV of AC signal was selected.

The impedance data is obtained and the graph is plotted. The polarization curves were obtained from -250 to 250 mV at OCP at a scan rate of 1 mVs⁻¹. The data is obtained and Tafel curves were plotted. From the i_{corr} value obtained corrosion rate is calculated using Eq 1:

$$\text{CR}(\text{mmy}^{-1}) = \frac{3.27 \times i_{\text{corr}} \times (\text{E.W.})}{D} \quad (\text{Eq 1})$$

where E.W. is the equivalent weight of the corroding species and D is the density of the corroding species in g cm⁻².

2.4 Scanning Electron Microscopy (SEM)

The surface morphology of EN18 steel and copper before and after annealing was determined using SEM after polishing using emery sheets and etching in NITAL (EN18 steel) and 5 g FeCl₃, 10 ml HCl, 50 ml glycerin, 30 ml DI Water by ASTM26 (copper). EVO MA18 at 5000 X magnification was utilized for obtaining the SEM images of annealed and as-

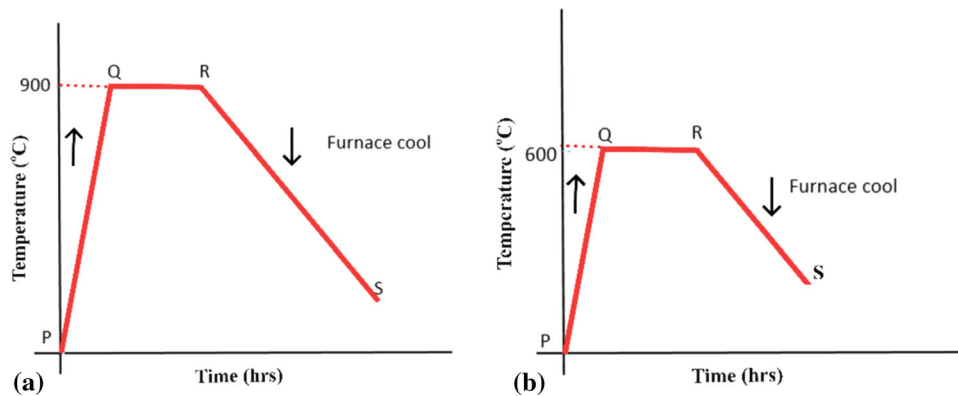


Fig. 1 Annealing heat treatment procedure for (a) EN18 steel (b) Copper

bought material. 1000 X magnification was used for SEM images for surface image capturing for polished and corroded sample analysis.

3. Results and Discussion

3.1 Potentiodynamic Polarization Studies (PDP)

The Tafel polarization technique was used to analyze the effect of annealing and the concentration of sulfuric acid on the corrosion behavior of EN 18 steel and copper. The Tafel plot was obtained for as-bought and annealed samples in different concentrations of the acid medium. The experiments were carried out in the temperature range of 30-50 °C . The plots obtained are given in Fig. 2 and 3. Various parameters such as corrosion current density (i_{corr}), corrosion potential (E_{corr}), cathodic slope ($-b_c$), and corrosion rate (CR) obtained by extrapolation of the cathodic curve for EN18 steel and copper are listed in Tables 2 and 3. It is observed that there is a curvature is seen in the anodic curve, which can be attributed to the passive oxide formation along with the dissolution of the metal at the higher anodic potential. This led to the calculation of various parameters such as E_{corr} and i_{corr} from the cathodic curve (Ref 24).

The results indicate that the corrosion rate increases with an increase in the concentration of the acid medium and temperature. With an increase in the concentration of sulfate ions, there is an increased tendency for the breakdown of the surface film formed by the corrosion product (Ref 25). The increase in the temperature leads to greater diffusion of ions and improvement in the electrochemical kinetics, which leads to a higher corrosion rate (Ref 26). When we compare the corrosion rate of EN18 steel and copper between as-bought and annealed samples in 0.5 M H_2SO_4 solution, it was found that the annealed sample shows a lesser corrosion rate than the as-bought one. In the case of iron, the volume fraction of the ferrite phase increases with annealing. The ferrite phases having more carbon content will act as an anode and pearlite act as a cathode, resulting in the formation of microgalvanic cells (Ref 27). The uniform distribution of the proeutectoid ferrite matrix containing the pearlite phases leads to greater contact between them. This leads to greater corrosion around the pearlite phase in the as-cast sample when compared to annealed samples. In the case of copper, it is due to the increase in grain size with

annealing, which leads to the creation of a blocking effect by the stabilized oxides due to an increase in the surface area within the grain boundaries, thus decreasing the access of ions to cause corrosion (Ref 20).

3.2 Corrosion Studies Using Electrochemical Impedance Spectroscopy (EIS)

The EIS method was employed to find the corrosion rate of EN18 steel and copper in various concentrations of H_2SO_4 solution for as-bought and annealed samples in different concentrations of the acid medium with a temperature variation of 30-50 °C. The Nyquist plot and Bodes plot obtained for EN18 steel and copper is given in Fig. 4 and 5, respectively. The plot is fitted with two different circuits (Fig. 6) for EN18 steel and copper due to the change in the nature of the curve. For both EN18 steel and copper, at high frequency, a depressed capacitive semicircle is observed. This is due to the charge transfer impedance (Ref 28). For copper, at low frequency, a straight line called Warburg impedance (W) is observed, which indicates diffusion of corrosion product from the surface of metal or reacting ion diffusion into the surface of copper (Ref 26). The one-time constant given by the Bodes plot indicates the presence of a single capacitive loop. The equivalent circuit consists of R_s (solution resistance), R_{ct} (the charge transfer resistance), and one constant phase element $Q1$ consisting of double-layer capacitance (CPE_{dl}) and deviation parameter (n_1). The substitution of the CPE_{dl} instead of the C_{dl} of an ideal capacitor is to account for the inhomogeneity arising on the surface of the metal. For copper, an additional element W is also added. The values of these parameters obtained for EN18 steel and copper are given in Tables 4 and 5. For this circuit, the polarization resistance (R_p) and the CPE_{dl} are calculated using the formula (Ref 29):

$$R_p = R_{ct} \quad (\text{Eq 2})$$

$$CPE_{dl} = \frac{Y_2 \omega^{n_2-1}}{\sin\left(\frac{n_2\pi}{2}\right)} \quad (\text{Eq 3})$$

where Y_2 and n_2 are the parameters of the constant phase elements Q_2 .

The difference in the R_{ct} value could be explained by the nature of the corrosion product formed. The corrosion product formed in the annealed EN18 steel and copper seems to be more insoluble and protective than the unannealed specimens,

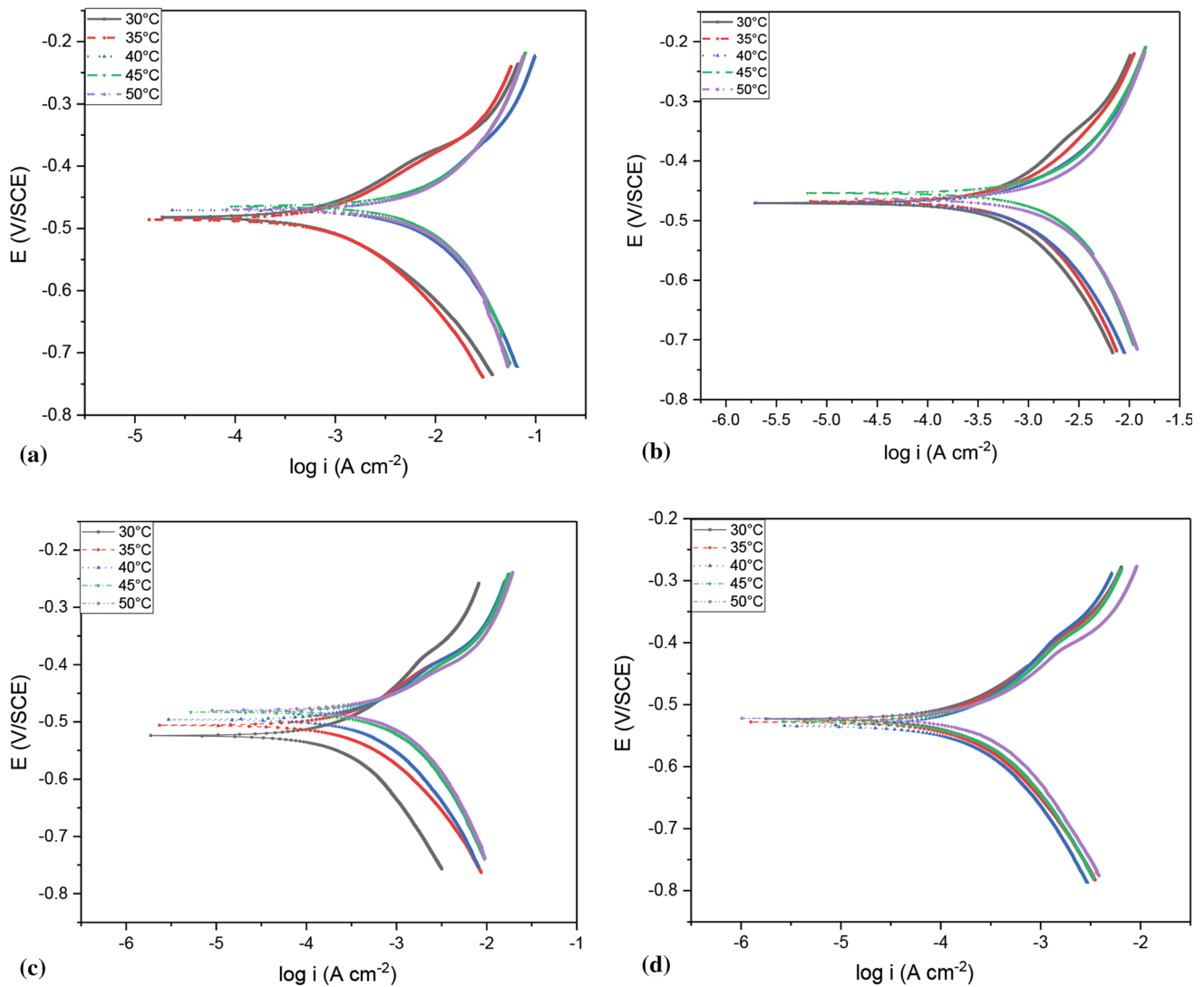


Fig. 2 Tafel plots for the corrosion of EN18 steel (a) before annealing in 0.5 M H₂SO₄ (b) after annealing (AA) in 0.5 M H₂SO₄ (c) AA in 0.25 M medium H₂SO₄ (d) AA in 0.1 M H₂SO₄ medium at different temperatures

whereas its formation is found to be prohibited with the sulfate attack with an increase in temperature and concentration. It is observed that the R_p values decrease with an increase in the temperature of the corrosion study due to the enhanced dissolution of the oxide film. Thus, the protective oxide layer becomes thinner and more porous resulting in an increased corrosion rate (Ref 30). There is a significant increase in the R_p value with annealing for both the metals at different temperatures of study which leads to a decrease in the corrosion rate for the annealed material. This can be attributed to the increase in the crystallite size of the metals with annealing. As the grain size increases, the surface area of the grain boundaries increases due to grain refinement. This makes the oxide film to be more stabilized and creates a blocking effect, which will prevent the diffusion of corrosive ions to come in contact with the surface of the metal. For both metals, irrespective of the concentration of the medium or after annealing treatment, the capacitive semicircle decreased with an increase in temperature. This suggests that there is an elevation in the corrosion with temperature for both metals. There is an increase in the R_p value with a decrease in the concentration of the medium of H₂SO₄,

which indicates that the rate of corrosion increases with an increase in concentration. This result is in accordance with results obtained from PDP studies. An increase in the R_p value, thus the decrease in the corrosion rate was observed after annealing.

3.3 Kinetic and Thermodynamic Parameters

An Arrhenius equation is used to calculate the activation energy of corrosion of EN18 steel and copper in an H₂SO₄ medium and the relation between the corrosion rate and the activation energy is given by (Ref 31) Eq 4.

$$CR = A \times \exp\left(\frac{E_a}{RT}\right) \quad (\text{Eq 4})$$

where CR is the corrosion rate of the reacting species, E_a is the activation energy, A is the pre-exponential factor and T is the absolute temperature. The log (CR) versus T plot for various concentrations of the medium and different annealing conditions is given in Fig. 7 and the parameters are represented in Table 6.

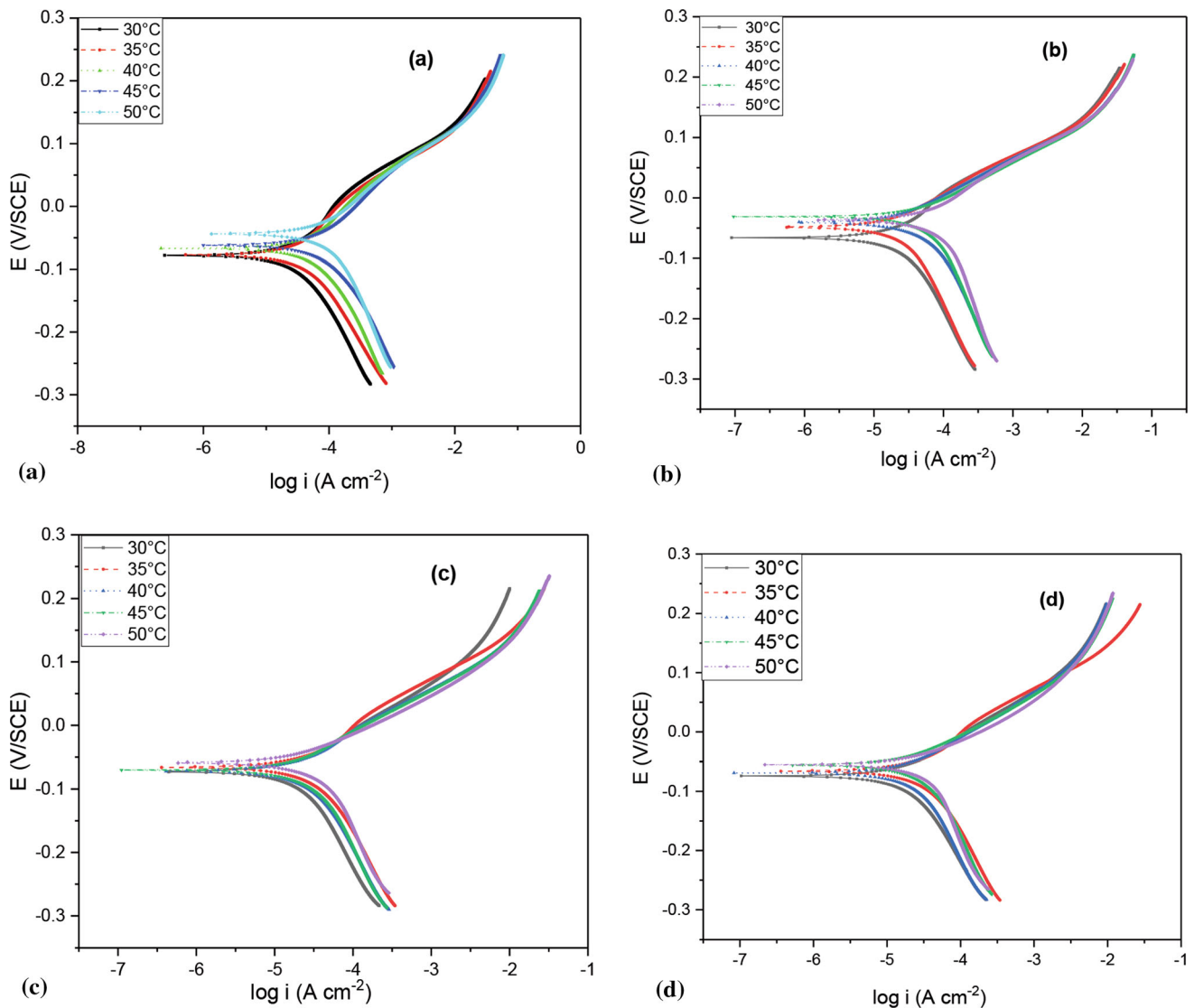


Fig. 3 Tafel plots for the corrosion of copper (a) before annealing in 0.5 M H₂SO₄ (b) after annealing (AA) in 0.5 M H₂SO₄ (c) AA in 0.25 M medium H₂SO₄ (d) AA in 0.1 M H₂SO₄ medium at different temperatures

From transition state theory, the enthalpy of activation (ΔH^\ddagger) and entropy of activation (ΔS^\ddagger) are calculated using (Ref 31):

$$CR = \frac{RT}{Nh} \exp\left(\frac{\Delta S^\ddagger}{R}\right) \exp\left(\frac{\Delta H^\ddagger}{RT}\right) \quad (\text{Eq 5})$$

where h is the Planck's constant, N is the Avogadro's number. ΔH^\ddagger and ΔS^\ddagger values are obtained from the slope and intercept of the plot ($\log(CR/T)$ vs. $1/T$) (Fig. 8) and are represented in Table 6.

The E_a value for both the metals at all the studied concentrations of the medium and annealing conditions is found to be greater than 20 KJ mol⁻¹. This confirms the surface-controlled corrosion mechanism (Ref 32). The E_a value increases with an increase in the concentration of the medium which indicates that E_a value is dependent on the activation polarization (Ref 30). The E_a value of the annealed metal is more than that of the as-cast metal which also indicates its dependence on the activation polarization.

The ΔS^\ddagger value is large and negative. This implies that the rate-determining step represents association indicating a reduction in the disorder in going from reactant to activated complex. There is a decrease in the ΔS^\ddagger value with acid concentration which suggests that the dissolution of metal is promoted by an increase in concentration (Ref 33).

3.4 SEM Analysis of EN18 Steel and Copper

The SEM analysis of EN18 steel and copper before and after annealing was performed and is given in Fig. 9 and 10, respectively. The light region in both the images represents pearlite and the dark region represents proeutectoid ferrite. Figure 9 represents the phases present in the as-bought condition. The fine pearlitic colony with well-dispersed proeutectoid ferrite is observed. The interlamellar distance between two different phases in pearlite is very small as compared to AISI 5140 steel in the annealed conditions. After annealing (Fig. 9b) coarser pearlite colonies as hatched regions are visible. The dark spaces between the needle represent the ferrite

Table 2 Results of PDP measurements for the corrosion of EN18 steel before and after annealing in H₂SO₄ medium

Metal	H ₂ SO ₄ , M	T, °C	E _{corr} , V versus SCE	i _{corr} , ×10 ⁻⁴ A cm ⁻²	-b _c , mV dec ⁻¹	CR, ×10 ⁻³ , mmy ⁻¹
EN18 steel before annealing	0.5	30	- 0.481	8.56 ± 0.26	8.09	9.93
		35	- 0.486	10.7 ± 0.67	6.95	12.4
		40	- 0.471	60.3 ± 0.85	5.36	69.8
		45	- 0.477	64.8 ± 3.78	4.78	75.1
		50	- 0.465	99.6 ± 2.76	4.40	115
EN18 steel after annealing	0.5	30	- 0.472	5.27 ± 1.57	5.60	6.11
		35	- 0.469	6.28 ± 1.25	5.18	7.29
		40	- 0.472	13.7 ± 0.2	5.09	8.01
		45	- 0.454	24.3 ± 0.58	4.31	16.6
		50	- 0.464	32.7 ± 2.2	4.37	17.1
EN18 steel after annealing	0.1	30	- 0.523	4.80 ± 0.01	5.30	3.54
		35	- 0.506	5.26 ± 0.29	6.97	3.74
		40	- 0.497	7.43 ± 0.41	6.03	5.54
		45	- 0.484	7.10 ± 0.22	5.30	8.82
		50	- 0.479	8.88 ± 0.31	5.30	9.60
EN18 steel after annealing	0.25	30	- 0.523	5.05 ± 0.76	6.34	2.08
		35	- 0.527	6.23 ± 0.06	6.37	2.62
		40	- 0.534	8.78 ± 1.07	6.08	2.82
		45	- 0.528	11.61 ± 0.51	5.80	2.43
		50	- 0.522	1.28 ± 0.17	5.70	3.33

Table 3 Results of PDP measurements for the corrosion of copper before and after annealing in H₂SO₄ medium

Metal	H ₂ SO ₄ , M	T, °C	E _{corr} , V versus SCE	i _{corr} , ×10 ⁻⁵ A cm ⁻²	-b _c , mV dec ⁻¹	CR, ×10 ⁻⁴ , mmy ⁻¹
Copper before annealing	0.5	30	- 0.078	1.59 ± 0.76	8.09	3.49
		35	- 0.077	2.44 ± 0.43	6.95	4.86
		40	- 0.064	5.74 ± 1.78	5.36	6.94
		45	- 0.062	7.61 ± 0.93	4.78	9.45
		50	- 0.044	28.2 ± 1.67	4.40	11.8
Copper after annealing	0.5	30	- 0.035	1.44 ± 0.84	5.60	2.71
		35	- 0.049	2.24 ± 0.06	5.18	2.79
		40	- 0.040	4.40 ± 1.25	5.09	6.65
		45	- 0.031	5.54 ± 0.14	4.31	7.37
		50	- 0.037	7.4 ± 1.3	4.37	11.1
Copper after annealing	0.25	30	- 0.073	2.34 ± 0.39	4.66	2.72
		35	- 0.065	2.47 ± 0.67	4.40	2.86
		40	- 0.075	2.74 ± 0.07	4.84	3.17
		45	- 0.070	2.99 ± 0.12	4.43	3.47
		50	- 0.058	3.41 ± 0.6	3.87	3.96
Copper after annealing	0.1	30	- 0.074	2.07 ± 0.02	5.19	2.40
		35	- 0.067	2.37 ± 0.05	4.51	2.75
		40	- 0.069	2.72 ± 0.11	4.40	3.15
		45	- 0.055	2.91 ± 0.56	4.51	3.37
		50	- 0.057	4.00 ± 0.59	3.20	4.64

phase. In normalizing or casting conditions, the degree of supercooling is higher than furnace cooling (annealing), and the rate of nucleation dominates that of the growth process to yield well-dispersed finer grains (colony) (Ref 34).

For copper, the microstructure exhibits lighter and darker regions in the as-cast substrate (Fig. 10a). This can be due to the curvature of the crystal lattice (Ref 35). After annealing, the contrast in the color has reduced, and resulting annealing twins are observed (Fig. 10b). There is an increase in the grain size with annealing, which can be attributed to the formation of the annealing twins (Ref 19).

The surface morphology of the freshly polished and corroded in 0.5 M H₂SO₄ of the as-cast EN18 steel and copper was determined using SEM and is given in Fig. 11. A uniform attack by the corrosive ions on the surface is observed for both the metals and the degradation is clearly visible. Few scratches due to polishing are visible on the freshly polished surface. The Energy-dispersive spectroscopy (EDS) spectra of the annealed EN18 and copper show the formation of an oxygen peak after immersion in the H₂SO₄ solution as shown in Fig. 12(b) and (d). This shows the presence of FeSO₄ in EN18 steel and oxygen due to the sulfate ion on the surface.

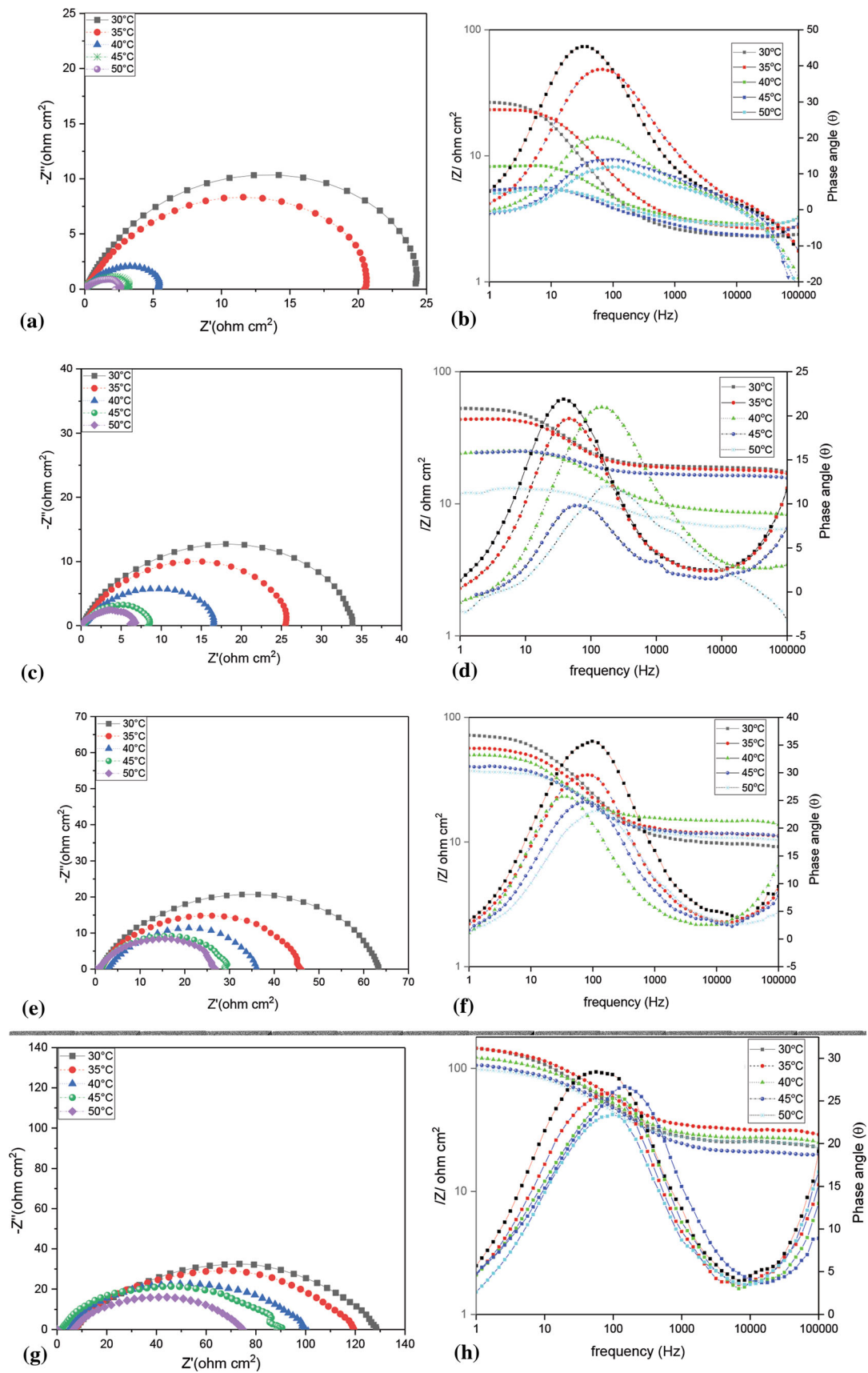


Fig. 4 Nyquist plots and Bode plots for the corrosion of EN18 steel (a), (b) before annealing in 0.5 M H₂SO₄ (c), (d) after annealing (AA) in 0.5 M H₂SO₄ (e), (f) AA in 0.25 M medium H₂SO₄ (g), (h) AA in 0.1 M H₂SO₄ medium at different temperatures

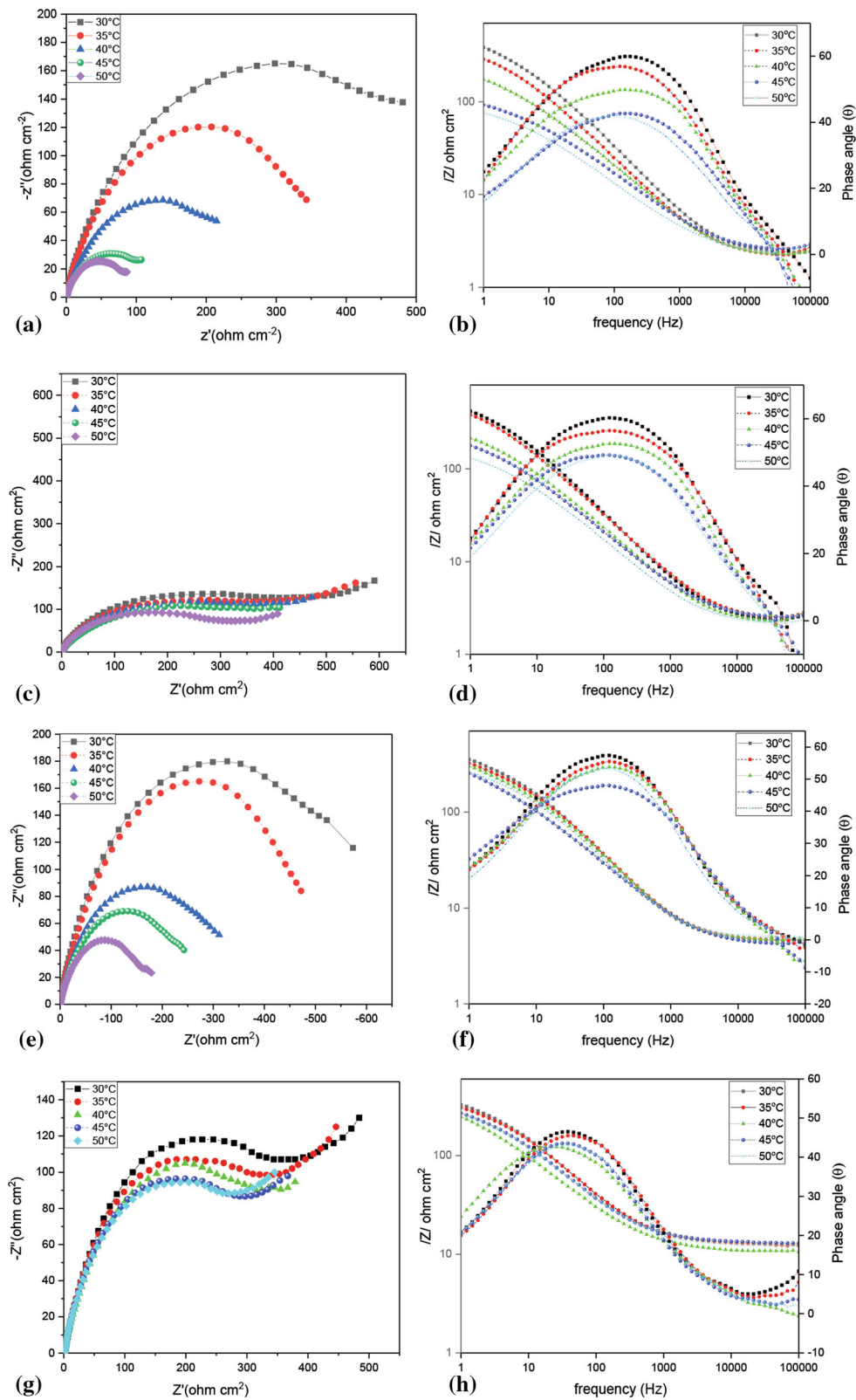


Fig. 5 Nyquist plots and Bode plots for the corrosion of copper (a), (b) before annealing in 0.5 M H₂SO₄ (c), (d) after annealing (AA) in 0.5 M H₂SO₄ (e), (f) AA in 0.25 M medium H₂SO₄ (g), (h) AA in 0.1 M H₂SO₄ medium at different temperatures

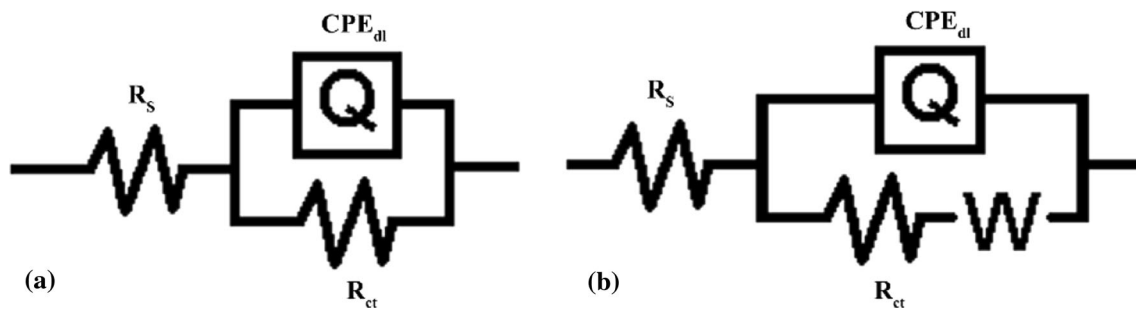


Fig. 6 Equivalent circuit of (a) EN18 steel (b) copper in H₂SO₄ medium

Table 4 Results of EIS measurements for the corrosion of EN18 steel before and after annealing in H₂SO₄

Metal	H ₂ SO ₄ , M	T, °C	R _s , Ω cm ²	CPE _{dl} , × 10 ⁻³	n	χ ² , × 10 ⁻³	R _{ct} , Ω cm ²
EN18 steel before annealing	0.5	30	2.39	3.25	0.84	1.40	25.34 ± 2.3
		35	2.75	3.50	0.80	1.41	21.59 ± 3.6
		40	2.99	3.72	0.79	1.43	5.52 ± 0.96
		45	2.95	3.76	0.73	1.24	5.57 ± 0.78
		50	2.85	3.93	0.76	1.09	2.60 ± 0.56
EN18 steel after annealing	0.5	30	19.02	0.81	0.86	0.22	34.78 ± 2.5
		35	18.52	0.91	0.85	0.31	26.20 ± 3.41
		40	8.70	1.24	0.79	0.73	17.18 ± 0.27
		45	6.64	7.91	0.90	0.30	8.44 ± 2.301
		50	6.54	2.57	0.71	0.88	3.70 ± 0.9
EN18 steel after annealing	0.25	30	9.52	1.52	0.77	1.49	64.07 ± 2.50
		35	11.50	1.51	0.78	1.30	46.77 ± 3.21
		40	14.83	1.54	0.83	3.70	36.54 ± 2.31
		45	11.53	1.59	0.83	1.21	29.73 ± 1.78
		50	10.61	2.12	0.75	0.61	27.21 ± 0.99
EN18 steel after annealing	0.1	30	24.06	4.23	0.69	4.81	130.10 ± 5.67
		35	30.69	4.29	0.69	3.27	121.50 ± 7.67
		40	26.11	4.35	0.69	2.53	100.20 ± 3.65
		45	19.74	5.43	0.66	1.48	90.36 ± 0.87
		50	24.46	5.55	0.66	4.31	75.84 ± 2.34

Table 5 Results of EIS measurements for the corrosion of copper before and after annealing in H₂SO₄ solution

Metal	H ₂ SO ₄ , M	T, °C	R _s , Ω cm ²	CPE _{dl} , × 10 ⁻⁵	n	χ ² , × 10 ⁻³	R _{ct} , Ω cm ²	W, × 10 ⁻² Ω ⁻¹ cm ² s ^{1/2}
Copper before annealing	0.5	30	2.28	4.73	0.75	3.43	448.30 ± 35.87	0.73
		35	2.28	6.90	0.74	1.08	356.80 ± 21.89	2.71
		40	2.19	10.5	0.68	3.80	210.00 ± 36.76	2.03
		45	2.56	17.2	0.65	1.12	98.48 ± 23.98	3.23
		50	2.47	24.3	0.66	1.62	81.35 ± 17.89	5.33
Copper after annealing	0.5	30	2.33	4.55	0.75	4.01	827.80 ± 20.20	0.99
		35	2.47	4.85	0.73	3.81	491.80 ± 43	2.73
		40	2.31	8.38	0.71	1.54	260.90 ± 35.9	1.83
		45	2.43	10.2	0.67	4.7	225.90 ± 34.78	3.14
		50	2.14	13.9	0.69	4.66	154.70 ± 23.89	4.86
Copper after annealing	0.25	30	4.41	4.64	0.76	1.74	394.40 ± 22.67	0.78
		35	4.43	4.74	0.74	2.23	355.50 ± 10.59	0.79
		40	4.47	5.10	0.73	4.11	325.40 ± 13.42	0.76
		45	4.02	5.29	0.66	3.94	334.20 ± 8.56	1.11
		50	4.75	6.14	0.73	1.66	291.90 ± 14.67	1.43
Copper after annealing	0.1	30	12.66	4.87	0.71	1.53	378.10 ± 6.78	0.95
		35	12.25	4.97	0.70	4.13	345.30 ± 20.25	0.97
		40	10.46	7.65	0.65	0.15	349.00 ± 12.21	1.77
		45	12.78	6.01	0.69	1.90	307.10 ± 18.92	1.16
		50	11.89	6.24	0.68	0.11	298.60 ± 21.21	1.07

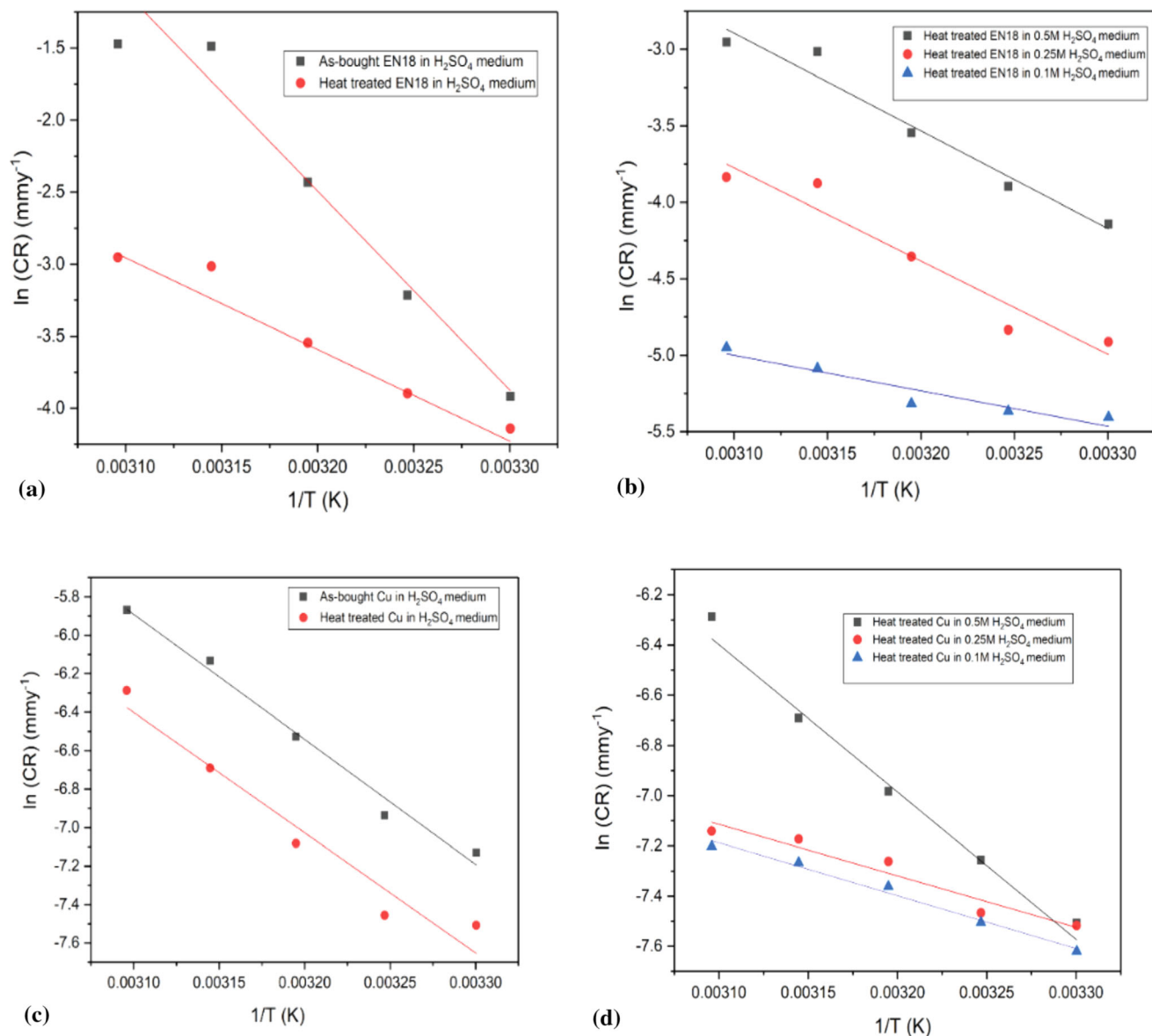


Fig. 7 Arrhenius plots of (a) EN18 steel (b) EN18 steel (c) Copper in 0.5 M H₂SO₄ medium for the corrosion in as-bought and annealed condition, and (d) Copper in different concentrations of H₂SO₄ medium in the annealed condition

Table 6 Activation parameters for the corrosion of EN18 steel and copper in H₂SO₄ medium within as-bought and annealed condition

Metal	Annealing treatment	H ₂ SO ₄ , M	E _a , KJ/mol	ΔH [#] , KJ/mol	ΔS [#] , J/mol/K
EN18 steel	Before	0.5	114.72	103.80	- 60.31
	After	0.5	52.94	50.34	- 119.90
	After	0.25	50.64	48.04	- 128.04
Copper	After	0.1	19.36	16.76	- 235.21
	Before	0.5	54.07	51.47	- 135.01
	After	0.5	51.99	49.39	- 145.72
	After	0.25	23.93	49.39	- 145.72
	After	0.1	15.36	14.93	- 259.07

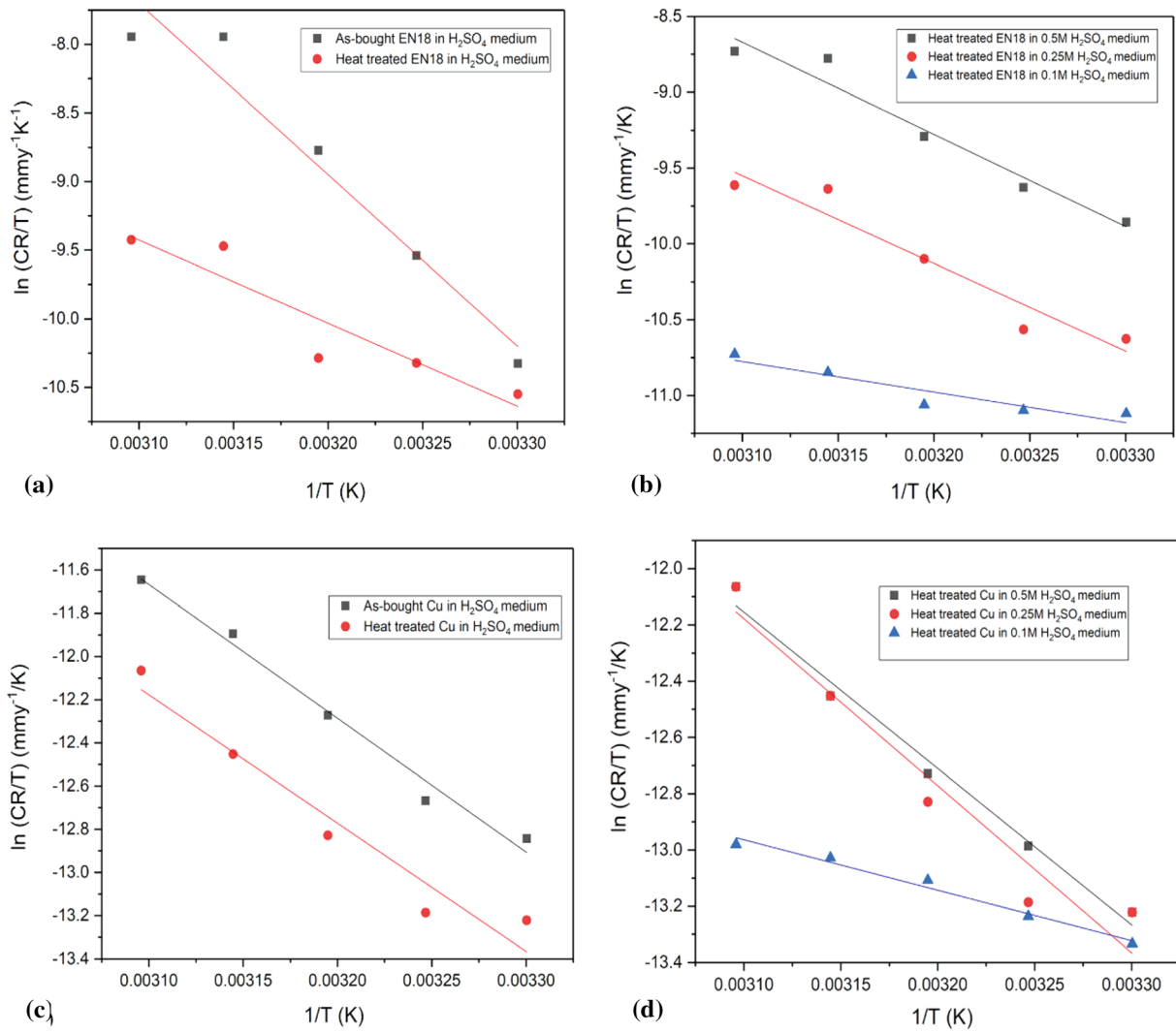


Fig. 8 Plots of $\ln(CR/T)$ versus $1/T$ of (a) EN18 steel (b) EN18 steel, (c) Copper in 0.5 M H₂SO₄ medium for the corrosion in as-bought and annealed condition and (d) Copper in different concentrations of H₂SO₄ medium in the annealed condition

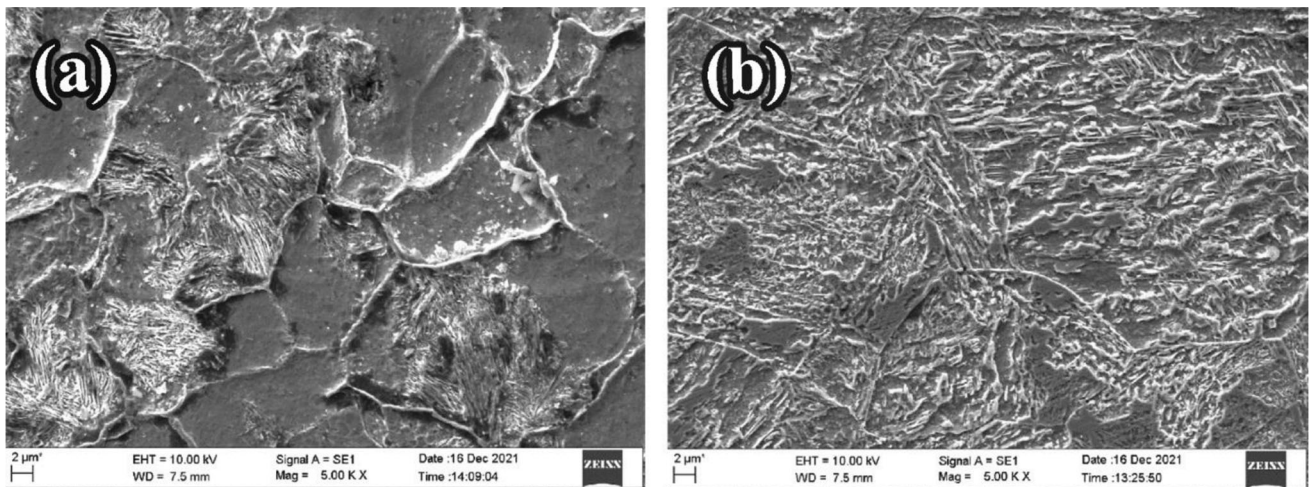


Fig. 9 SEM images of EN18 steel (a) before and (b) after annealing at 900 °C

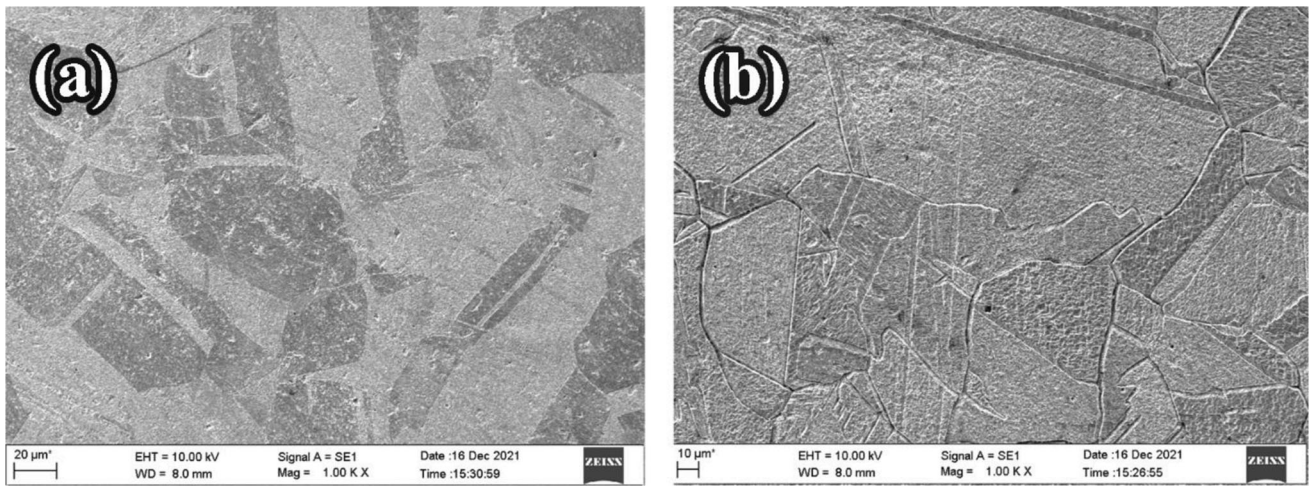


Fig. 10 SEM images of copper (a) before and (b) after annealing at 600 °C

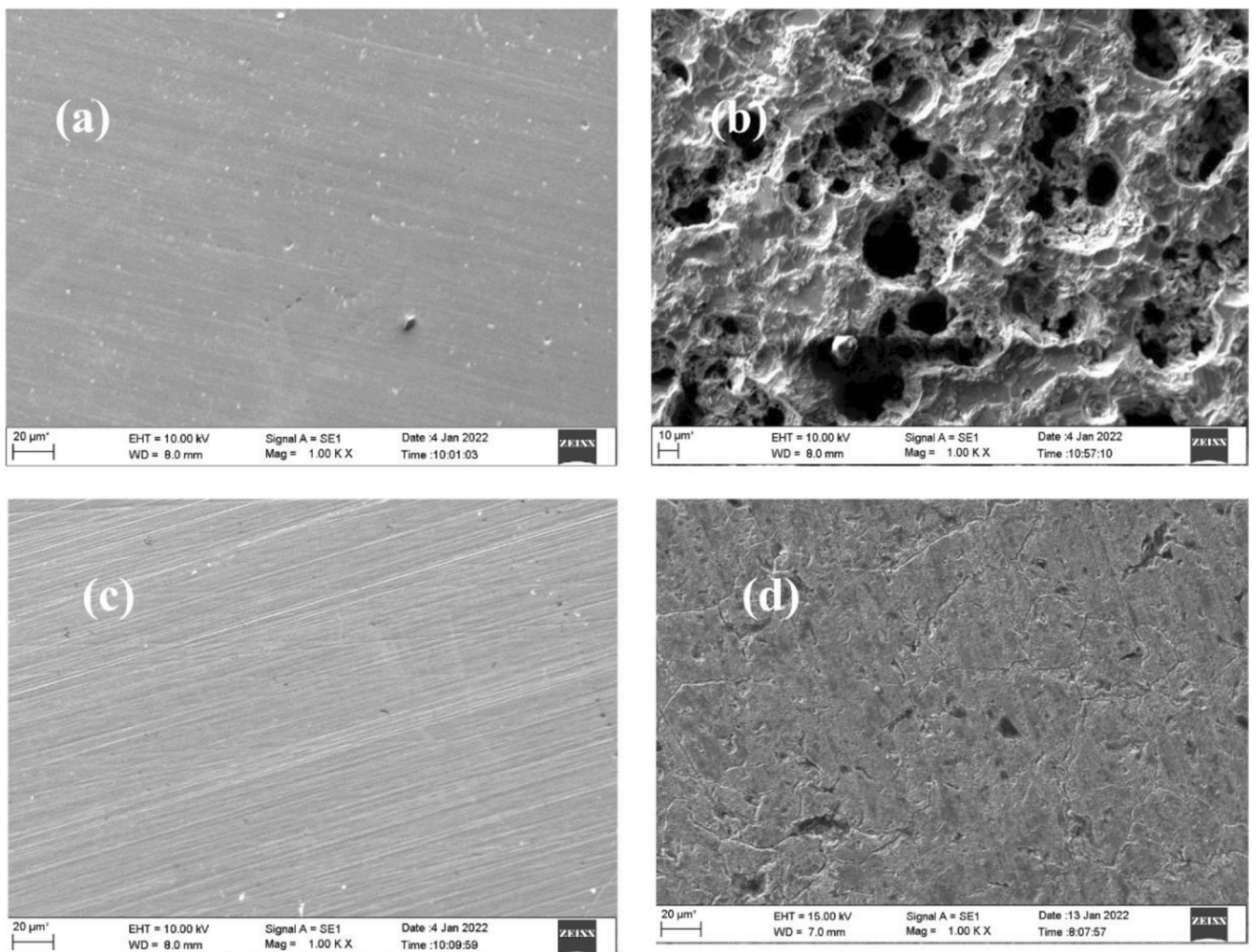


Fig. 11 SEM images of (a) freshly polished EN18 steel (b) EN18 steel after immersion in 0.5 M H₂SO₄ medium, (c) freshly polished copper (d) copper after immersion in 0.5 M H₂SO₄ medium

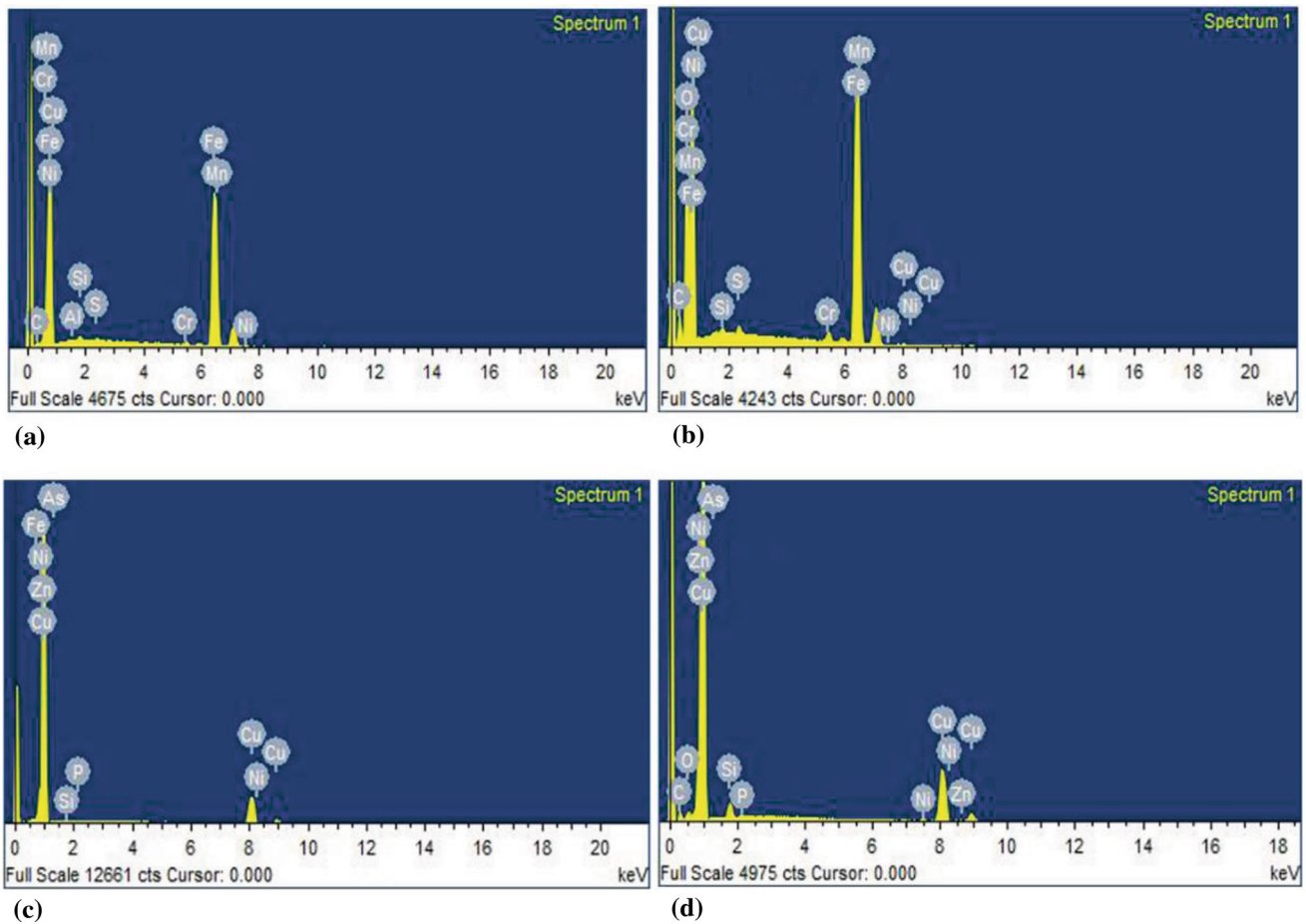


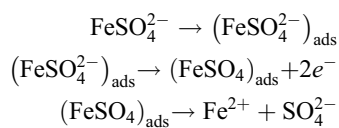
Fig. 12 EDS spectra of (a) freshly polished EN18 steel (b) EN18 steel after immersion in 0.5 M H₂SO₄ medium, (c) freshly polished copper (d) copper after immersion in 0.5 M H₂SO₄ medium

3.5 Mechanism of Corrosion

From the literature, the corrosion mechanism involved in EN18 steel and copper H₂SO₄ is discussed. The cathodic reaction mechanism of EN18 steel and copper in H₂SO₄ solution involves two steps, that is oxygen and hydrogen reduction. The cathodic reaction involves the formation of H₂O, and H₂. The equation representing these are as follows (Ref 36)

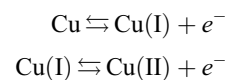
1. Reduction in hydrogen : $H^+ + 2e^- \rightarrow H_2$
 Oxygenreduction : $O_2 + 2e^- + 4H^+ \rightarrow 2H_2O$
2. $O_2 + 2e^- + 2H^+ \rightarrow H_2O_2$
 $H_2O_2 + 2e^- + 2H^+ \rightarrow 2H_2O$

The anodic reaction mechanism of EN18 steel in H₂SO₄ solution is as follows (Ref 36):



(FeSO₄)_{ads} formed at the metal surface diffuses to the bulk solution, which leads to the dissolution of metal.

The anodic reaction mechanism of copper in an H₂SO₄ medium takes place in two continuous steps:



The rate of the second step is slower, so the corrosion process is governed by the formation of Cu(II).

4. Conclusions

This work discusses the influence of annealing treatment on the microstructure and corrosion behavior of EN18 steel and copper in an H₂SO₄ medium. From the results, the following conclusions are given below:

1. EN18 steel and copper undergo corrosion in an H₂SO₄ medium, the corrosion rate increases with an increase in the concentration of acid for both the annealed materials.
2. EIS and PDP studies displayed that there is an increase in the corrosion resistance after annealing of the metals.
3. The corrosion rate increases with an increase in temperature for as-bought and annealed materials of EN18 steel and copper.

- The surface morphology determined using SEM of the corroded samples confirms the intensity of corrosion on the surface of the metal and the EDS measurements determine the composition of elements present on the surface of metal before and after corrosion.
- Suitable corrosion mechanism for both EN18 steel and copper in an H₂SO₄ medium has been discussed.

Acknowledgments

The authors acknowledge the laboratory and characterization facilities extended by the Department of Chemistry, Department of Mechanical & Manufacturing Engineering and Central Instrumentation Facility, Manipal Institute of Technology (MIT), Manipal, Manipal Academy of Higher Education (MAHE). Ms. Jilna Jomy is grateful to MAHE, Manipal, for awarding the Dr. TMA Pai scholarship.

Funding

Open access funding provided by Manipal Academy of Higher Education, Manipal. The authors received intramural funding from the Manipal Academy of Higher Education, Manipal to carry out the research work.

Data Availability

Inquiries about data availability should be directed to the corresponding author.

Conflict of interest

On behalf of all authors, the corresponding author claims no conflict of interest.

Open Access

This article is licensed under a Creative Commons Attribution 4.0 International License, which permits use, sharing, adaptation, distribution and reproduction in any medium or format, as long as you give appropriate credit to the original author(s) and the source, provide a link to the Creative Commons licence, and indicate if changes were made. The images or other third party material in this article are included in the article's Creative Commons licence, unless indicated otherwise in a credit line to the material. If material is not included in the article's Creative Commons licence and your intended use is not permitted by statutory regulation or exceeds the permitted use, you will need to obtain permission directly from the copyright holder. To view a copy of this licence, visit <http://creativecommons.org/licenses/by/4.0/>.

References

- R. Solmaz, E. Altunbaşşahin, A. Döner, and G. Kardaş, The Investigation of Synergistic Inhibition Effect of Rhodanine and Iodide Ion on the Corrosion Of Copper in Sulphuric Acid Solution, *Corr. Sci.*, 2011, **53**, p 3231–3240.
- M.N. El-Haddad, Inhibitive Action and Adsorption Behavior of Cefotaxime Drug at Copper/Hydrochloric Acid Interface: Electrochemical, Surface and Quantum Chemical Studies, *RSC Adv.*, 2016, **6**, p 57844–57853.
- B. Tan et al., Insight into the Corrosion Inhibition of Copper in Sulfuric Acid via Two Environmentally Friendly Food Spices: Combining Experimental and Theoretical Methods, *J. Mol. Liq.*, 2019, **286**, p 110891.
- J. Zhang, L. Zhang, and G. Tao, A Novel and High-Efficiency Inhibitor of 5-(4-methoxyphenyl)-3h-1,2-dithiole-3-Thione for Copper Corrosion Inhibition in Sulfuric Acid at Different Temperatures, *J. Mol. Liq.*, 2018, **272**, p 369–379.
- B. Tan et al., Experimental and Theoretical Studies on the Inhibition Properties of Three Diphenyl Disulfide Derivatives on Copper Corrosion in Acid Medium, *J. Mol. Liq.*, 2020, **298**, p 111975.
- D. Clover, B. Kinsella, B. Pejčić, and R. de Marco, The Influence of Microstructure on the Corrosion Rate of Various Carbon Steels, *J. Appl. Electrochem.*, 2005, **35**, p 139–149.
- S. I. Ao, C. Douglas, W. S. Grundfest, and J. Burgstone, Microstructural Features and Mechanical Behavior of Unalloyed Medium Carbon Steel After Subsequent Heat Treatment. In: Proceedings of the world congress on Engineering and Computer Science 1107 (2014)
- O. Abedini, M. Behroozi, P. Marashi, E. Ranjbarnodeh, and M. Pouranvari, Intercritical Heat Treatment Temperature Dependence of Mechanical Properties and Corrosion Resistance of Dual Phase Steel. *Mater. Res.* 22 (2019)
- M.C. Bignozzi et al., Effect of Heat Treatment Conditions on Retained Austenite and Corrosion Resistance of the X190CrVMo20-4-1 Stainless Steel, *Met. Mater. Int.*, 2020, **26**, p 1318–1328.
- Q. Zhang, Q. Li, and X. Chen, Effect of Heat Treatment on Corrosion Behavior of Mg–5Gd–3Y–0.5Zr Alloy, *RSC Adv.*, 2020, **10**, p 43371–43382.
- D. Prabhu, S. Sharma, P.R. Prabhu, J. Jomy, and R.V. Sadanand, Analysis of the Inhibiting Action of Pectin on Corrosion of AISI1040 Dual-Phase Steel with Ferrite–Martensite and Ferrite–Bainite Structure: A Comparison in 0.5 M Sulphuric Acid, *J. Iran. Chem. Soc.*, 2021, **19**, p 1109–1128.
- F.F. Eliyan, E.-S. Mahdi, and A. Alfantazi, Electrochemical Evaluation of the Corrosion Behaviour of API-X100 Pipeline Steel in Aerated Bicarbonate Solutions, *Corros. Sci.*, 2012, **58**, p 181–191.
- X. Wang, X. Tang, L. Wang, C. Wang, and Z. Guo, Corrosion Behavior of X80 Pipeline Steel under Coupling Effect of Stress and Stray Current, *Int. J. Electrochem. Sci.*, 2014, **9**, p 4574–4588.
- O.O. Daramola, B.O. Adewuyi, and I.O. Oladele, Effects of Heat Treatment on the Mechanical Properties of Rolled Medium Carbon Steel, *J. Miner. Mater. Charact. Eng.*, 2010, **9**, p 693–708.
- Y.S. Lim, J.S. Kim, S.J. Ahn, H.S. Kwon, and Y. Katada, The Influences of Microstructure and Nitrogen Alloying on Pitting Corrosion of Type 316L and 20 wt.% Mn-Substituted Type 316L Stainless Steels, *Corros. Sci.*, 2001, **43**, p 53–68.
- T.V. Shibaeva, V.K. Laurinavichyute, G.A. Tsirlina, A.M. Arsenkin, and K.V. Grigorovich, The Effect of Microstructure and Non-Metallic Inclusions on Corrosion Behavior of Low Carbon Steel in Chloride Containing Solutions, *Corros. Sci.*, 2014, **80**, p 299–308.
- C. Zhang, D. Cai, B. Liao, T. Zhao, and Y. Fan, A Study on the Dual-Phase Treatment of Weathering Steel 09CuPcNi, *Mater. Lett.*, 2004, **58**, p 1524–1529.
- Y. Kayali and B. Anaturk, Investigation of Electrochemical Corrosion Behavior in a 3.5wt.% NaCl Solution of Boronized Dual-Phase Steel, *Mater. Des.*, 2013, **46**, p 776–783.
- D.P. Field, L.T. Bradford, M.M. Nowell, and T.M. Lillo, The Role of Annealing Twins during Recrystallization of Cu, *Acta Mater.*, 2007, **55**, p 4233–4241.
- G. Palumbo et al., Effect of Grain Size on the Corrosion Behavior of Fe-3wt.%Si-1wt.%Al Electrical Steels in Pure Water Saturated with CO₂, *Materials*, 2021, **14**, p 5084.
- Y. Zhao, I.C. Cheng, M.E. Kassner, and A.M. Hodge, The Effect of Nanotwins on the Corrosion Behavior of Copper, *Acta Mater.*, 2014, **67**, p 181–188.
- O. Keleştemur and S. Yıldız, Effect of Various Dual-Phase Heat Treatments on the Corrosion Behavior of Reinforcing Steel used in the Reinforced Concrete Structures, *Constr. Build. Mater.*, 2009, **23**, p 78–84.

23. P.K. Katiyar, S. Misra, and K. Mondal, Comparative Corrosion Behavior of Five Microstructures (Pearlite, Bainite, Spheroidized, Martensite, and Tempered Martensite) Made from a High Carbon Steel, *Metall Mater. Trans. A*, 2019, **50**, p 1489–1501.
24. M.A. Amin et al., Microstructure and Corrosion Behaviour of Carbon Steel and Ferritic and Austenitic Stainless Steels in NaCl Solutions and the Effect of p-Nitrophenyl Phosphate Disodium Salt, *Int. J. Electrochem. Sci.*, 2016, **11**, p 10029–10052.
25. N. Dinodi and A. NityanandaShetty, Electrochemical Investigations on the Corrosion Behaviour of Magnesium Alloy ZE41 in a Combined Medium of Chloride and Sulphate, *J. Magnes. Alloys*, 2013, **1**, p 201–209.
26. H. Li et al., Investigation of Losartan Potassium as an Eco-Friendly Corrosion Inhibitor for Copper in 0.5 M H₂SO₄, *J. Mol. Liquids*, 2020, **305**, p 112789.
27. A. Rodríguez-Torres, O. Olivares-Xometl, M.G. Valladares-Cisneros, and J.G. González-Rodríguez, Effect of Green Corrosion Inhibition by Prunus Persica on AISI 1018 Carbon Steel in 0.5M H₂SO₄, *Int. J. Electrochem. Sci.*, 2018, **13**, p 3023–3049.
28. Y. Gong, Z. Wang, F. Gao, S. Zhang, and H. Li, Synthesis of New Benzotriazole Derivatives Containing Carbon Chains as the Corrosion Inhibitors for Copper in Sodium Chloride Solution, *Ind. Eng. Chem. Res.*, 2015, **54**, p 12242–12253.
29. P.D. ReenaKumari, J. Nayak, and A. NityanandaShetty, Corrosion Behavior of 6061/Al-15 vol pct SiC(p) Composite and the Base Alloy in Sodium Hydroxide Solution, *Arab. J. Chem.*, 2016, **9**, p S1144–S1154.
30. D. Prabhu, Adsorption and Inhibition Action of a Novel Green Inhibitor on Aluminium and 6063 Aluminium Alloy in 1.0 M H₃PO₄ Solution, *Proc. Mater. Sci.*, 2014, **5**, p 222–231.
31. P. Deepa and R. Padmalatha, Corrosion Behaviour of 6063 Aluminium Alloy in Acidic and in Alkaline Media, *Arab. J. Chem.*, 2017, **10**, p S2234–S2244.
32. A.M. Abdel-Gaber, E. Khamis, H. Abo-ElDahab, and S. Adeel, Inhibition of Aluminium Corrosion in Alkaline Solutions using Natural Compound, *Mater. Chem. Phys.*, 2008, **109**, p 297–305.
33. S.I. Al-Rubaiey, E.A. Anoon, and M.M. Hanoon, The Influence of Microstructure on the Corrosion Rate of Carbon Steels, *Eng. Tech. J.*, 2013, **31**, p 1825–1836.
34. W. Cai and P. Bellon, Effect of Annealing Treatment on the Dry Sliding Wear Behavior of Copper, *Wear*, 2019, **426**, p 1187–1194.
35. K. Krishnaveni and J. Ravichandran, A Study on the Inhibition of Copper Corrosion in Sulphuric Acid by Aqueous Extract of Leaves of Morinda Tinctoria, *J. Fail. Anal. Prev.*, 2015, **15**, p 711–721.
36. A. Al-Moubaraki, A. Ganash, and S.D. Al-Malwi, Investigation of the corrosion behavior of mild steel/H₂SO₄ systems, *Moroc. J. Chem.*, 2020, **8**, p 264–279.

Publisher's Note Springer Nature remains neutral with regard to jurisdictional claims in published maps and institutional affiliations.